Applied Catalysis B: Environmental 110 (2011) 58–70

Contents lists available at SciVerse ScienceDirect

Applied Catalysis B: Environmental

journal homepage: www.elsevier.com/locate/apcatb

Catalytic reduction of nitrates in water on Pt promoted Cu hydrotalcite-derived catalysts: Effect of the Pt–Cu alloy formation

A. Aristizábal[a], S. Contreras[a,*], N. Barrabés[b,1], J. Llorca[c], D. Tichit[b], F. Medina[a]

[a] Departament d'Enginyeria Quimica, Universitat Rovira i Virgili, Campus Sescelades, Av. Països Catalans 26, 43007, Tarragona, Spain
[b] Institut Charles Gerhardt UMR 5253 CNRS/UM2/ENSCM/UM1, Matériaux Avancés pour la Catalyse et la Santé, 8 rue Ecole Normale, 34296 Montpellier Cedex 5, France
[c] Institut de Tècniques Energètiques i Centre de Recerca en Nanoenginyeria, Universitat Politècnica de Catalunya, Diagonal 647, 08028 Barcelona, Spain

ARTICLE INFO

Article history:
Received 20 April 2011
Received in revised form 2 August 2011
Accepted 18 August 2011
Available online 25 August 2011

Keywords:
Catalytic hydrogenation of nitrates
Hydrotalcite
Alloy formation
Pt–Cu

ABSTRACT

In this work, the role of the Pt–Cu interaction and the influence of the Pt metal loading in the catalytic reduction of nitrates in water have been studied, using Pt supported on CuMgAl mixed oxides catalysts in a continuous reactor. Following three Pt impregnation protocols different surface chemistries were obtained, as confirmed by BET, TPR, HRTEM, XRD and FTIR spectroscopy. In the first protocol, the presence of Cu and Pt–Cu alloy formation has been promoted, whereas the second protocol leads to separated Pt and Cu particles in close contact. The third protocol leads to the presence of Cu, Pt and Pt–Cu alloy particles. The different catalytic behaviors were related to the differences in the surface metal chemistry of the samples. Low ammonium formation was detected in all cases but nitrite concentrations need to be improved to fulfill the maximum admissible concentration of the EU legislation. It is concluded that: (i) the presence of Pt–Cu alloy particles leads to an increase in nitrogen selectivity, enhancing the nitrite reduction but showing lower nitrate conversion, and (ii) to maximize the nitrate conversion it is necessary to obtain mainly Pt particles interacting with Cu and Pt–Cu alloy particles.

1. Introduction

Groundwater pollution with high nitrate concentration represents an environmental problem worldwide [1]. Nitrate is a potential human health hazard, and drinking water standards were established by the governments to prevent health problems like clinical cyanosis [2,3]. Different techniques to remove nitrate from water had received attention [4–6] like catalytic reduction of nitrates [7,8], reverse osmosis [9], ion-exchange [10] and biological treatment [11,12]. The catalytic reduction of nitrates is one of the most eco-friendly technologies because it transforms nitrates into nitrogen and water [13]. This process using a bimetallic catalysts and hydrogen was firstly described by Vorlop and Tacke [14,15]. Different catalytic systems combining a noble metal (Pt or Pd) and a promoting metal (like Cu or Sn), supported on several materials, have been studied extensively for this reaction [16–22]. Their main drawback is the formation of ammonia and nitrite which are undesirable in drinking water and due to this recent studies in catalytic reduction of nitrates have been focused in the optimization of the activity and selectivity toward nitrogen formation ([23] and references herein). The incidence of several parameters of the process, such as reactor type [24,25], type of reducing agent [13,26], pH [27,28], and of the catalyst, such as synthesis method [19,29,30] and nature of the bimetallic pair [31], have been extensively studied. The surface chemistry of the metals [29] and the nature of the support [17,32,33] have shown to be key parameters in the optimization of the nitrogen formation.

The surface metal chemistry plays an important role in the catalytic reduction of nitrates, and the nature of the active sites (that can be tuned by the synthesis method) is crucial for the catalytic activity and selectivity. Due to this the clear identification of the optimal chemical state of the metals and the active sites nature is important to clarify the reaction mechanism involved, in order to optimize nitrogen selectivity and to determine the best synthesis method. Previous works have been focused in Pd–Cu or Pt–Cu bimetallic catalysts, and it is stated that this is a structure-sensitive process [34,35]. It has been clearly established that monometallic Pd or Pt particles are active sites to reduce nitrite selectively to nitrogen, and can reduce nitrate but at very low rate or are practically inactive [19,36]. Also, Yoshinaga et al. [35] suggested that edge and corner sites of Pd are active sites for ammonia formation while nitrogen is favorably formed on the terrace sites of the Pd crystallites. Due to these, to enhance the nitrogen selectivity it is necessary to avoid these active sites, for example, by

* Corresponding author. Tel.: +34 977559680; fax: +34 977559621.
E-mail address: sandra.contreras@urv.cat (S. Contreras).
[1] Current address: Institute of Materials Chemistry, Vienna University of Technology, Getreidemarkt 9, A-1060 Vienna, Austria.

0926-3373/$ – see front matter © 2011 Elsevier B.V. All rights reserved.
doi:10.1016/j.apcatb.2011.08.024

depositing atoms of another metal like copper in the edges and corners of the Pd particles. Furthermore, in order to increase the activity for nitrate reduction, a second non noble metal (like copper) is necessary, but its addition affects the nitrite reduction adversely in terms of selectivity to nitrogen [36]. To maintain the activity of the non noble metal (probably by spillover of hydrogen), a good contact with the noble metal is required [35]. Sá et al. [19] suggested that the promoter (non noble metal) is stabilized by the noble metal, and that this stabilization is due to the close contact between the metals that could be improved by an adequate synthesis method or by alloy formation. The alloy formation in the catalysts has been reported in several bimetallic systems [19,35–37] but in few cases is directly related to the catalytic behavior. Soares et al. [37] suggested that in order to obtain high activities the metals must be in close contact but not alloyed. Nevertheless, the influence of the metals interaction is still not clear and the changes in the catalytic behavior as a function of the alloy formation are still not fully understood.

On the other hand, the nature of the support, particularly its adsorptive capability, is of major importance to overcome diffusion limitations, which affect the kinetics and the selectivity of the reaction [24,25,33,38]. As it was demonstrated by Palomares et al. [33], calcined hydrotalcite-type materials could be an adequate catalyst support with high adsorption capacity for this reaction due to its peculiar reconstruction ability. Besides, different surface Pt states have been previously reported for Pt impregnated hydrotalcite-type catalysts [39] varying the Pt impregnation protocol. Hydrotalcites (HT) or layered double hydroxides compounds can be represented by the general formula: $[M(II)_{1-x}M(III)_x(OH)_2]^{x+}[(A_{x/n}{}^{n-})]\cdot mH_2O$, where x is typically between 0.25 and 0.33, and A^{n-} is a n-valent interlayer anion. These compounds present positively charged brucite-like layers, $Mg(OH)_2$, with trivalent cations M(III) substituting divalent cations M(II) in octahedral sites. Upon calcination, they form homogeneous mixed metal oxides. Besides, reduction of the metal cation-containing ones generally leads to a high dispersion of the metallic crystallites. Depending on the nature of the cations, the mixed oxides can recover the initial lamellar structure when rehydrated in water. This property is generally called "memory effect" [40]. Catalysts obtained from Cu-containing HT precursors show high dispersion of copper [32,41]. Different types of HT have been used as catalyst supports for the reduction of nitrates in water [28,42,43]. Palomares et al. [32,33] found that Pd supported over CuMgAl calcined HT catalyst is more active and selective toward nitrogen in the reduction of nitrates than Pd–Cu/Al_2O_3 due to the higher copper dispersion and the reconstruction ability of the HT which reduces the diffusion limitations. Besides, Wan et al. [22] observed that the nitrite selectivity and the activity of the same type of catalysts is directly related to the adsorption capacity. The studies carried out with HTs as catalysts for nitrate removal have not been performed in a packed bed continuous reactor (PBR) and Pt was not used as noble metal until a recent study published by our group [44]. Pt instead of Pd has been chosen because Pt has been successfully used as noble metal for this reaction with other kinds of supports [16,45].

In order to contemplate how the surface metal chemistry affects the activity and selectivity in the nitrate reduction, catalysts obtained from CuMgAl HTs impregnated by different protocols with Pt have been synthesized and tested. Copper selected as the promoting metal was introduced during the formation of the HT phase by co-precipitation, obtaining after calcination small and highly dispersed CuO particles. The presence of Mg and Al cations in the HT structure will increase the reconstruction ability of the materials. Three different Pt impregnation protocols have been followed, looking for different Pt sites on the surface (as reported previously in [39]). The materials have been characterized by temperature programmed reduction (TPR), X-ray powder diffraction (XRD), infrared spectroscopy (IR), high resolution transmission electron microscopy (HRTEM) and nitrogen adsorption, in order to correlate physico-chemical properties with the catalytic activity in the nitrate reduction.

2. Experimental

2.1. Characterization techniques

Elemental chemical analysis of Cu, Mg and Al in the calcined hydrotalcite was determined by ICP spectroscopy. 0.5 g of sample was dissolved in 5 ml of HNO_3, and then it was diluted to 25 ml with distilled water. Also the Pt content of the different catalysts was determined.

Powder X-ray diffraction (XRD) patterns were measured using a Bruker-AXS D8-Discover diffractometer with parallel incident beam (Gobel mirror) and vertical θ–θ goniometer, a 0.02° receiving slit and scintillation counter as detector. The angular 2θ diffraction range was between 5° and 70°. The data were collected with an angular step of 0.05° at 3 s per step. Cu-Kα radiation was obtained from a copper X-ray tube operated at 40 kV and 40 mA. X-ray patterns were compared to X-ray powder references to confirm phase identities using the Joint Committee on Powder Diffraction Standards (JCPDS, 2006) files.

The BET surface area of the catalysts and the calcined HT materials was determined in a Micromeritics ASAP 2010 apparatus, from the nitrogen adsorption isotherms at 77 K. Prior to the analysis the samples were degasified 5 h at 120 °C.

Temperature programmed reduction (TPR) analyses were performed in a TPD/R/O 1100 (ThermoFinnigan) equipped with a thermal conductivity detector (TCD). The reduction process was carried out between 30 °C and 900 °C, with a heating rate of 10 °C/min and with a flow rate of 20 ml/min of the reducing gas mixture (5% H_2 in argon).

High-resolution transmission electron microscopy (HRTEM) was performed with a JEOL 2010F instrument equipped with a field emission source (point-to-point resolution 0.19 nm, resolution between lines 0.14 nm). Samples were dispersed on holey-carbon coated grids from ultrasonicated alcohol suspensions.

FT/IR analysis of the catalysts and the used catalysts were performed in a FT/IR-680 plus Jasco using an ATR-300/H Serie diamond detector with a measurement range of 4000–60 cm^{-1}. The analyses were performed with a resolution of 2 cm^{-1} and 32 scan times. Before the analysis the used catalysts were dried at 100 °C.

Chemical analysis of copper and platinum in the treated water was determined by atomic absorption spectroscopy (HITACHI Z-8200 Polarized Zeeman Atom Absorption Spectrophotometer). The samples were preserved with concentrated nitric acid.

2.2. Catalyst synthesis

A CuMgAl HT with molar ratios Mg/Cu = 1 and (Mg + Cu)/Al = 3 was prepared by co-precipitation at room temperature. An aqueous solution containing $Mg(NO_3)_2\cdot 6H_2O$, $Al(NO_3)_3\cdot 9H_2O$ and $Cu(NO_3)_2\cdot 3H_2O$ in adequate amounts, and a second solution of sodium hydroxide (NaOH, 2 M) were slowly and simultaneously added to a beaker containing Milli-Q water under vigorous stirring. The pH value was maintained around 10 by NaOH (1 M) addition. The suspension was aged at room temperature under stirring overnight. The resulting solid, labelled as HT, was then filtered and washed several times with Milli-Q water. The solid was calcined at 450 °C overnight and labelled as HTcal.

Then, Pt was incorporated into the HTcalc support (0.5% or 1 %wt.) by three different protocols in order to obtain different interactions between Cu and the noble metal as previously

Table 1
Reactor and reaction conditions during catalytic tests.

Parameter	Value
Mass of catalytic bed	0.5 or 1 g
Catalytic bed height	0.5 or 1 cm (depending on the catalysts weight)
Reaction temperature	25 °C
Operating pressure	1 bar
Gas flow rate	3 ml/min
Liquid flow rate	1.2 ml/min
Nitrate feed concentration	100 mg/l
Reactor material	Stainless steel
Reactor configuration	H_2 and nitrate solution are feed to the reactor in co-current flow
Reactor internal diameter	1 cm

reported by Barrabés et al. [39] (protocol R and WR are described herein), where the same materials were used obtaining different catalytic behaviors in the in the gas-phase hydrodechlorination of trichloroethylene. Dihydrogen hexachloroplatinate (IV) hydrate (H_2PtCl_6) was used as Pt precursor in all cases.

Protocol R: HTcalc was reduced under 7 ml/min of hydrogen for 3 h at 350 °C. After reduction, the sample was put in contact with an ethanol solution containing H_2PtCl_6, and stirred at room temperature for one night under argon atmosphere. Then, the solid was centrifuged, and the precipitate was dried at 100 °C. Finally, calcination was performed for 2 h at 300 °C. These catalysts were labelled as R(0.5) and R(1), the value in parenthesis indicating the Pt metal loading (%wt).

Protocol WR: The second synthesis protocol is analogue to the first one, omitting the reduction step before the noble metal introduction. These catalysts were labelled as WR(0.5) and WR(1).

Protocol DI: Catalysts WR(0.5) and R(0.5) were again impregnated (as described for protocol WR) with an ethanol solution containing H_2PtCl_6 until the total amount of Pt reaches 1%wt referred to the support weight. These double impregnated catalysts were labelled as WR(0.5/0.5) and R(0.5/0.5).

2.3. Catalysts testing

The catalysts were tested for the catalytic reduction of nitrates, in a tubular packed bed continuous reactor using hydrogen as reducing agent. The reactor was packed with the catalyst (in order to obtain different residence times, different catalyst weights were tested), and was fed with hydrogen flow and with a nitrate solution ca. 100 ppm ($NaNO_3$) in Milli-Q water. Table 1 presents the reaction conditions and the description of the catalytic system.

All catalysts were reduced at 300 °C under hydrogen flow (7 ml/min) for 2 h before the catalytic tests.

The conversion and selectivities calculated are defined as:

$$X_{\text{Nitrate}} = \frac{(C_{\text{initial}} - C_{\text{final}})}{C_{\text{initial}}} \cdot 100 \quad (1)$$

$$S_i = \frac{\text{moles of } i \text{ produced/L}}{\text{moles of nitrate converted/L}} \cdot 100 \quad (2)$$

$$S_{\text{Nitrogen}}{}^{*} = 100 - S_{\text{Nitrite}} - S_{\text{Ammonium}} \quad (3)$$

where X_{Nitrate} is the nitrate conversion at 300 min. C_{final} is concentration of nitrates in the effluent at 300 min of reaction time. C_{initial} is initial concentration of nitrates feed to the reactor (ca. 100 ppm). S_i is selectivity toward product *i*. *i* is the nitrites, nitrogen or ammonium. * No other intermediate products have been detected in liquid and gas phase.

To determine the catalytic activity and the adsorption capacity of the support (CuMgAlOx, mixed oxide), three different tests were performed, using 0.5 g of the support packed in the reactor:

Test 1: The support was reduced at 300 °C under hydrogen flow (7 ml/min) like the catalysts. Then, a nitrate solution of 100 ppm was fed to the system in presence of 3 ml/min hydrogen flow to check if the support had some catalytic activity by its own.

Test 2: The support was reduced at 300 °C under hydrogen flow (7 ml/min) like the catalysts. Then, a nitrate solution of 100 ppm was fed to the system but in this case no hydrogen was fed into the reactor.

Test 3: After packing the support, a nitrate solution of 100 ppm was fed to the system but in this case no hydrogen was fed to the reactor and the reduction step was omitted.

Aqueous samples from the reactions were analyzed by HPLC. An anion separation column (Shodex IC SI-90 4E) for suppression method was used to determine the nitrate and nitrite concentration. A Shodex IC YK-421 column was used to analyze ammonium concentration.

3. Results and discussion

3.1. Characterization results

3.1.1. Elemental analysis

The elemental composition of the CuMgAl hydrotalcite precursor was determined by atomic absorption. The Cu/Mg and (Cu + Mg)/Al molar ratios were experimentally determined and are presented in Table 2, including the theoretical values for comparison. It can be seen that the experimental values are quite similar to the expected values. The results show that the copper content in the sample was around 0.38 g Cu per gram of sample in the CuMgAl calcined hydrotalcite.

Also, the Pt content of the catalysts was determined by ICP and in all cases similar values to the expected (1 and 0.5%) were obtained.

3.1.2. XRD and FTIR

The XRD patterns of the as-synthesized and calcined samples are shown in Fig. 1. The HT precursor exhibits reflections at 10.7°, 20.9°, 34.7°, 39.1°, 46°, 60.7° and 62°, typical of the hydrotalcite-like structure (JCPDS file No. 01-089-0460).

After calcination at 450 °C of the HT precursor, the hydrotalcite-like phase disappears leading to a mixture of $Mg(Al)O_x$ mixed oxides, and of tenorite (CuO) phase giving the characteristic diffraction peaks at $2\theta = 35.8°$ and 39° (JCPDS file No. 00-048-1548) (Fig. 1). These results are in agreement with previous works [39,46]. In all cases, the broader diffraction lines obtained indicate poor crystallinity of CuO phase.

The Pt-containing materials exhibit similar XRD patterns. Diffraction lines corresponding to Pt are not observed due to its small loading. Fig. 1 shows the XRD profiles of the representative fresh and used (after reaction) R(0.5/0.5) catalyst. For the fresh catalyst, copper oxide is the main crystalline phase. Furthermore, a small and broad diffraction line indicating the presence of Cu phase

Table 2
Elemental composition and molar ratios of the CuMgAl hydrotalcite precursor.

Hydrotalcite precursor	mol% Cu[a]	mol% Mg[a]	mol% Al[a]	Cu/Mg	(Cu+Mg)/Al
CuMgAl	39.2 (37.5)	*35.5* (37.5)	*25.3 (25)*	*1.1* (1)	*2.96* (3)

Theoretical values are given in parentheses.
[a] Concentrations are normalized to the total metal content.

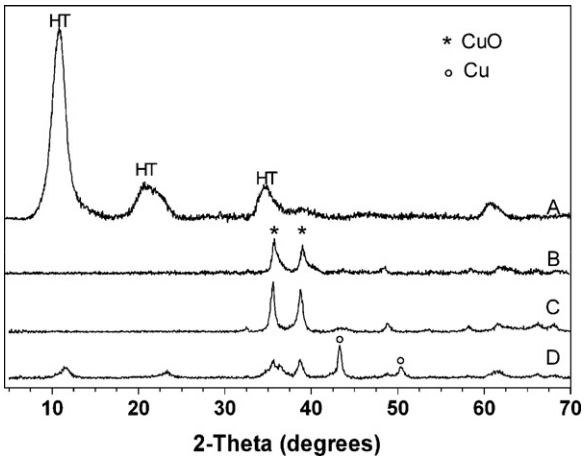

Fig. 1. Powder X-ray diffraction patterns of: (A) CuMgAl hydrotalcite precursor, (B) HTcal, (C) R(0.5/0.5) fresh catalysts, and (D) R(0.5/0.5) used catalyst.

is also detected (JCPDS 01-070-3038). For the used R(0.5/0.5) catalyst, a partial reconstruction of the mixed oxide support into the HT phase is observed in agreement with the behavior observed by Palomares et al. [33]; however the degree of reconstruction is very low. Furthermore, an increase of the Cu phase at the expense of the CuO phase is also observed for the used R(0.5/0.5) catalyst.

The reconstruction of the lamellar structure is also evidenced in the FTIR results. Fig. 2 shows typical IR spectra of fresh and used R(0.5/0.5) catalyst, which is representative of the other samples. The broad bands at 3410 and 1636 cm^{-1} present in all the spectra are assigned to the OH vibration modes of the structural OH groups and of the interlayer water molecules.

After contacting the materials with water during the reaction, the IR spectra of the samples presented an increase in the band of around 3410 cm^{-1} and new peaks between 1230 and 1450 cm^{-1}, not observed for the fresh materials, indicating a partial reconstruction of the hydrotalcite phase due to the memory effect. This could be assigned to the stretching N–O vibration of nitrates [33]. However, the presence of carbonates in the interlayer could not be discarded, and might be responsible of the shoulder observed at the band of ca. 1500 cm^{-1}. The small band observed at ca. 1250 cm^{-1} and 1185 cm^{-1} could be assigned to nitrites.

3.1.3. Textural properties

The textural properties of the different catalysts and of HTcalc reported in Table 3 show that they exhibit similar specific surface areas and pore volumes ranging from 74 to 98 m^2/g and from 0.21 to 0.26 cm^3/g, respectively. Therefore, differences in the catalytic

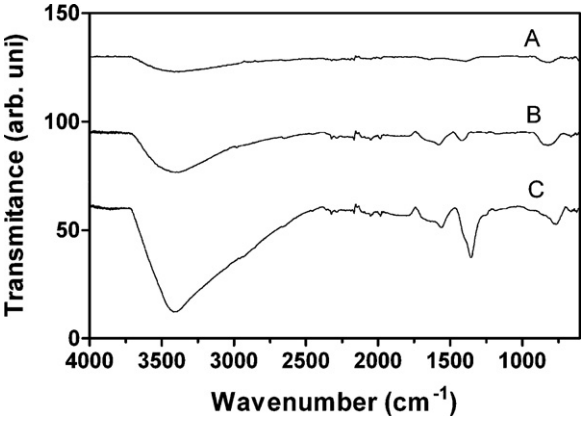

Fig. 2. IR spectra of: (A) HTcalc, (B) R(0.5/0.5) and (C) R(0.5/0.5) used catalysts.

Table 3
Surface areas and porosity of the samples.

Sample	S (m^2/g)	Pore volume (cm^3/g)	Average pore size (Å)
Cu/Mg/Al	79.2	0.23	83.5
R(0.5)	74.6	0.22	87.1
R(1)	92.6	0.26	87.4
R(0.5/0.5)	81.4	0.22	79.9
WR(0.5)	75.9	0.21	82.1
WR(1)	74.9	0.22	87.0
WR(0.5/0.5)	97.9	0.23	65.5

behavior should be more likely related to the interaction of the particles.

3.1.4. Reducibility by H_2-TPR

The reduction properties of the copper oxides from the fresh and used samples were examined by H_2-TPR. The results for the fresh and used catalysts are shown in Fig. 3. For fresh samples, the HTcalc sample (without Pt) shows a broad reduction peak around 290 °C, with two components around 280 °C and 300 °C. The first peak is attributed to the reduction of the highly dispersed copper oxide species and the second to the reduction of bulk CuO particles [39]. The addition of the noble metal increases the CuO reducibility and a shift to lower reduction temperatures is observed for all the samples. However, due to the high copper content respect to the Pt amount the peaks are just slightly shifted.

Differences in the TPR analyses of the materials due to the Pt incorporation protocols and the platinum amount are observed. The samples R(1) and WR(1) have a slight shift to lower reduction temperatures compared to R(0.5) and WR(0.5) samples, due to their higher platinum content. Also, samples prepared by R protocol (R(0.5) and R(1)) presented a small shift to higher reduction temperatures compared to WR samples at the same Pt metal loading. This is related to the different Pt and Cu interactions formed in each synthesis protocol, confirmed by HRTEM (see Section 3.1.4). Furthermore, catalysts R(0.5/0.5) and WR(0.5/0.5), presented two reduction peaks, which could be attributed to copper–platinum particles and to isolated copper for the lower and higher reduction peaks, respectively. In all samples no reduction peaks assignable to isolated PtO species were observed; Pt is in close contact with Cu or forming an alloy after the calcination step and no PtO was detected. Furthermore, for all the samples, the hydrogen consumption is mainly due to CuO, because a high Cu/Pt molar ratio (195.8 and 97.9 mol Cu/mol Pt for 1%Pt and 0.5%Pt metal loadings, respectively) is present in all catalysts.

According to the TPR results, the catalysts were reduced at 300 °C before the catalytic tests, because at this temperature the main part of the reducible species would be in the metallic form.

After the reaction, the samples were also analyzed by H_2-TPR, and changes in the samples with respect to the fresh catalysts are evidenced. After reaction, there is a segregation of the CuO phase in the used HTcalc catalyst; two peaks are identified at 287 °C and at 425 °C. Also, two peaks are observed in all the used catalyst (except for R(0.5/05)) but the position of the peaks and the ratio between them in each sample differ, suggesting that the catalysts stabilization of the CuO phase changes with the Pt content and the synthesis protocol used. The first peak identified in the samples is mainly due to well dispersed and stable copper oxide species in contact with Pt or Pt–Cu alloy, while the second peak is attributed to bulk CuO. Contrary to the rest of the samples, R(0.5/0.5) catalyst only shows one reduction peak centered at 265 °C, an intermediate T_{max} compared to both peaks observed in the fresh sample at 253 °C and 309 °C. Comparing catalysts prepared by the same protocol, it could be said that when the Pt loading decreases the phase segregation increases, indicating that part of the CuO phase is not in

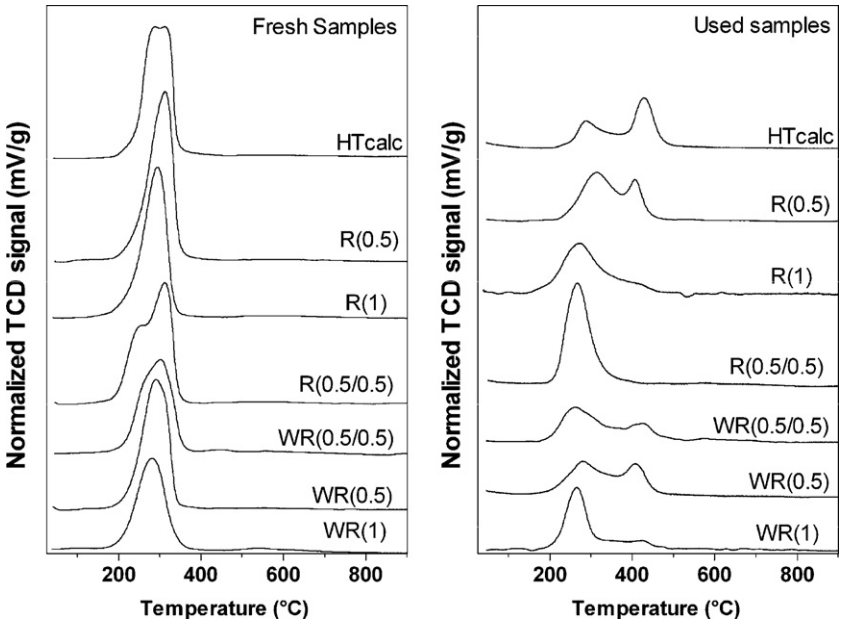

Fig. 3. TPR profiles of the fresh and used samples.

contact with Pt (as confirmed by HRTEM). The changes in the H_2-TPR profiles after reaction could indicate that some of the copper is oxidized during the reaction, and part of the CuO phase formed is not in contact with the Pt particles (as evidenced in the HRTEM) and as a consequence some part of the copper species are deactivated to reduce nitrates.

Hydrogen consumption calculated from the H_2-TPR data are presented in Table 4. As reference material CuO standard was selected.

The hydrogen consumption for the fresh CuMgAl, R(0.5) and R(1) catalysts, show very small differences and the values of hydrogen consumption are quite similar than the expected values taking into consideration the amount of copper in the samples. However for the WR catalysts some changes are observed. The hydrogen consumption was around 10% lower than the expected values, probably due to the exposure of the sample to hydrogen at room temperature before starting the TPR experiment. It seems that for these WR samples a part of the copper is reduced at room temperature. This fact was confirmed by XPS results (not shown). This is probably due to the presence of isolated Pt particles (observed by HRTEM) in close contact with CuO, which facilitates the reduction of copper oxide by hydrogen spillover from Pt. This effect is also observed in lower extent for the R(0.5/0.5) sample. It is important to note that this effect is not observed for the R(0.5) and R(1) catalysts that only contain Pt–Cu alloy particles.

For the used catalysts this trend is also maintained. The WR catalysts showed the lowest hydrogen consumption. These results indicate that during the reaction some part of the copper is oxidized and that the amount of oxidized copper depends on the synthesis protocol of the catalysts.

Table 4
Hydrogen consumption for fresh and used catalysts.

Sample	H_2, TPR (mmol/g)	
	Fresh catalysts	Used catalysts
CuMgAl	6.0	3.8
R(0.5)	6.0	3.5
R(1)	5.9	3.4
R(0.5/0.5)	5.7	3.2
WR(0.5)	5.6	3.0
WR(1)	5.4	2.8
WR(0.5/0.5)	5.3	2.9

3.1.5. HRTEM

The fresh CuMgAl support and the reduced catalysts were analyzed by HRTEM in order to determine the distribution, size and state of the metallic particles after reduction.

Fig. 4A shows two representative images of the CuMgAl sample at different magnification. The support is comprised by small particles ranging from 2 to 20 nm in size. Larger particles are likely due to Mg–Al–O, whereas smaller particles are CuO. Fig. 4B shows a HRTEM image where several of such particles are clearly visible. They are well dispersed over the support and exhibit lattice fringes at 2.54 Å, which corresponds to the (0 0 2) spacing of monoclinic CuO. The size distribution of CuO particles is very narrow and centered at about 2.2 nm.

Figs. 5 and 6 show the HRTEM images of the catalysts prepared by Protocol R (R(0.5) and R(1), respectively). Fig. 5A shows a representative low-magnification view of sample R(0.5), which mainly comprise particles in the range of 1.8–2.4 nm in size; some metal particles are marked by arrows. In Fig. 5B two individual metal particles of about 1.9 nm in diameter are identified along with HT layers oriented along the [1 0 0] crystallographic direction. The inset shows an enlargement of one of the particles, with a (1 1 1) lattice spacing value of 0.219 nm. A lattice fringe image of one of these particles is depicted in Fig. 5C and D. Spots at 0.218 nm in the corresponding Fourier Transform (FT) image are ascribed to (1 1 1) crystallographic planes and are indicative of solid solution formation between Pt and Cu. In addition to Cu–Pt alloy nanoparticles, the sample also contains particles of about 8–10 nm in diameter, which correspond to pure Cu.

Fig. 6 shows the images of sample R(1). It is comprised by well-dispersed metal particles, between 2.1 and 4.0 nm in diameter. Fig. 6A shows a representative image with some particles marked by arrows. The homogeneity of the sample merits to be highlighted. In addition, the lattice spacing values exhibited by all particles analyzed indicate that they correspond to the Pt–Cu alloy. Fig. 5B shows a HRTEM image of various metal crystallites along with a detailed enlarged lattice fringe image of one of them. The lattice

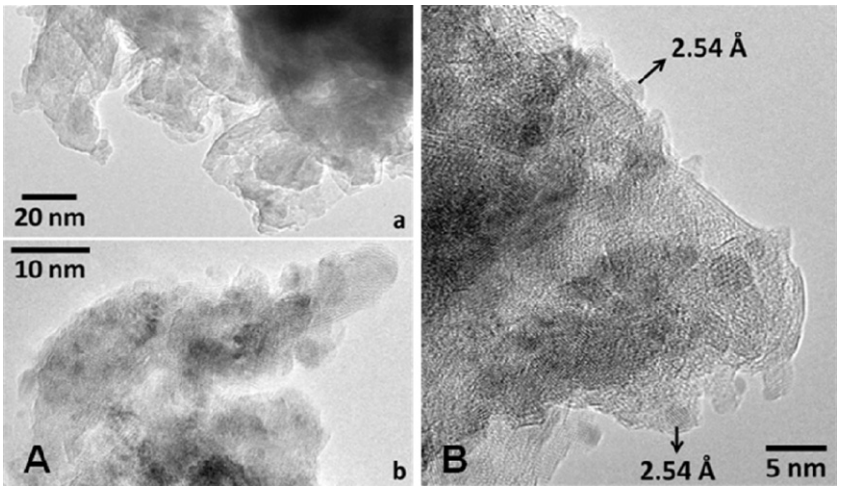

Fig. 4. Representative TEM and Lattice fringe images of CuMgAl support.

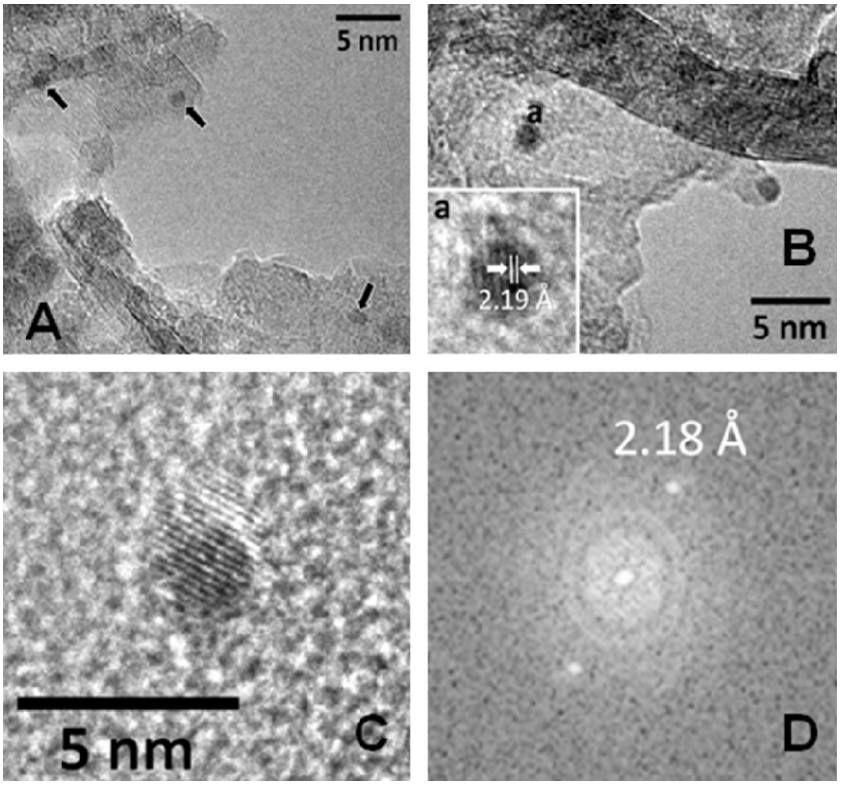

Fig. 5. Representative TEM and Lattice fringe images of catalyst R(0.5).

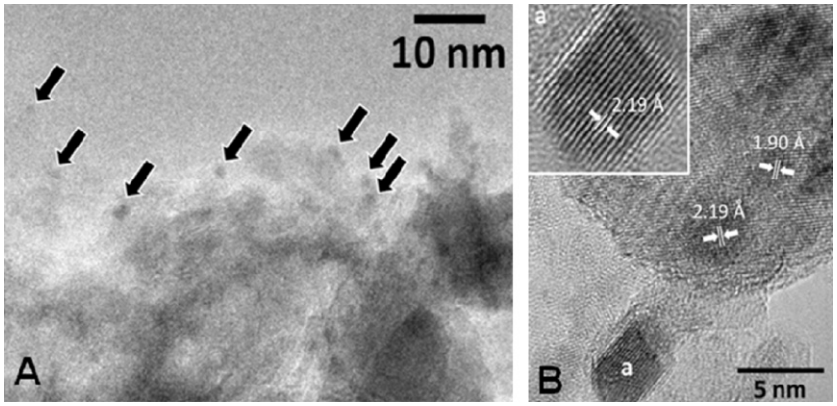

Fig. 6. TEM and HRTEM images of sample R(1).

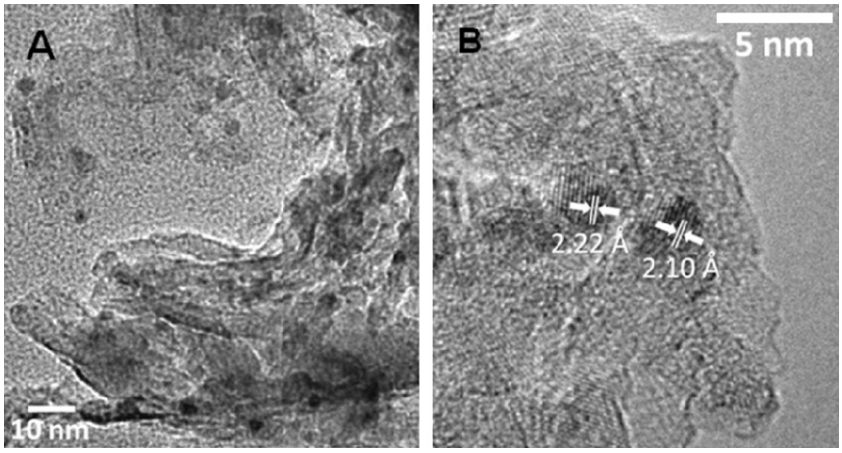

Fig. 7. TEM image of sample WR(0.5).

fringes recorded over various particles at 0.219 and 0.19 nm are ascribed to (1 1 1) and (2 0 0) crystallographic planes of Cu–Pt alloy, respectively. The sample also contains particles of about 8–10 nm in diameter which correspond to pure Cu.

Therefore, catalysts prepared by Protocol R (R(0.5) and R(1)) are mainly comprised by Pt–Cu alloy nanoparticles and by larger Cu particles of 8–10 nm.

Also, samples prepared by Protocol WR (WR(0.5) and WR(1)) were analyzed by HRTEM. These samples (not reduced before Pt incorporation) present different surface characteristics compared to those reduced before Pt impregnation discussed above. Fig. 7 shows a characteristic TEM image of sample WR(0.5); it contains particles with a size distribution between ca. 1.4 and 4 nm in diameter and also larger particle (of about 10 nm in diameter). The lattice fringe analysis of individual particles indicates that larger particles correspond to metallic Cu (0.209 nm), whereas the smallest particles can be identified with Pt nanoparticles (0.227 nm). Although the presence of alloy particles in this sample cannot be completely ruled out, it appears from HRTEM analysis that the sample is mainly comprised by separate Cu and Pt entities.

Sample WR(1) (see Fig. 8) contains metal particles of about 5–10 nm in diameter. A detailed analysis by HRTEM reveals that most particles in the range 5–6 nm correspond to pure Pt whereas some extent of Pt–Cu alloy was also detected. The particles around 10 nm correspond to Cu. This is shown in Fig. 8A and B, where lattice fringes at 0.228 and 0.220 nm are ascribed to (1 1 1) crystallographic planes of Pt and Pt–Cu alloy (Fig. 7A), respectively. In Fig. 8B, the lattice spacing at 0.209 nm recorded over a larger particle (of about 10 nm in diameter) corresponds well to the (1 1 1) crystallographic plane of metallic Cu.

It can be concluded that by the Protocol WR mainly Cu and Pt isolated particles are formed, although the presence of some extent of Pt–Cu alloy cannot be discarded.

Furthermore, we performed a TEM study of the materials prepared by double impregnation (Protocol DI), without reduction of the parent catalysts before the second impregnation with Pt. Following this protocol we expected to obtain different types and distributions of metallic particles in the surface of the catalysts. These samples (R(0.5/0.5) and WR(0.5/0.5)) were analyzed by HRTEM in order to confirm the hypothesis.

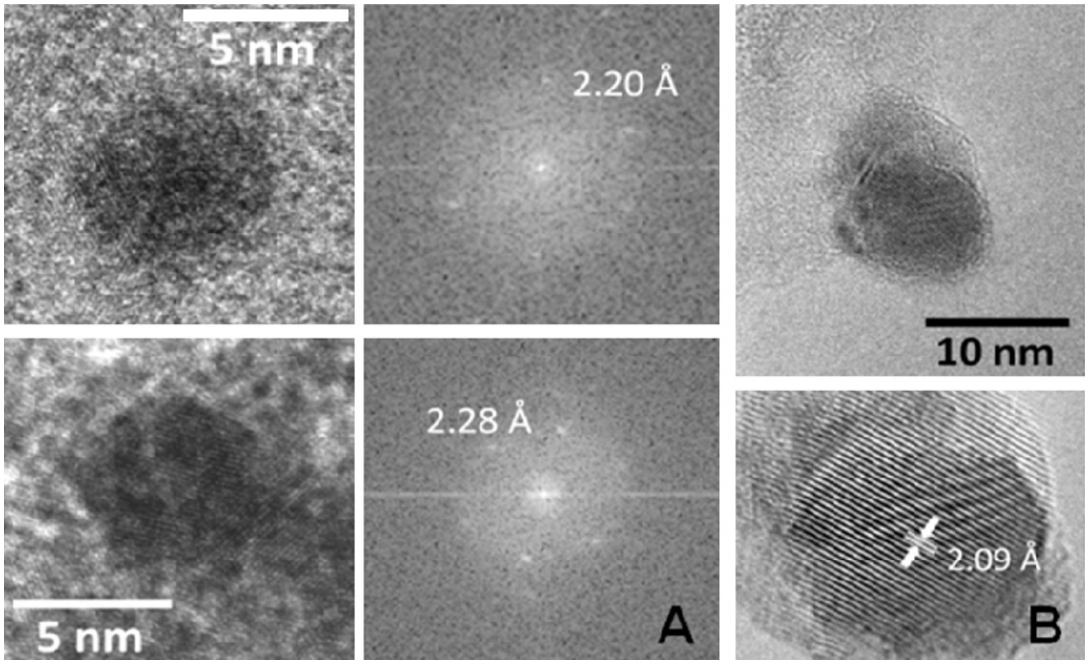

Fig. 8. HRTEM image of sample WR(1).

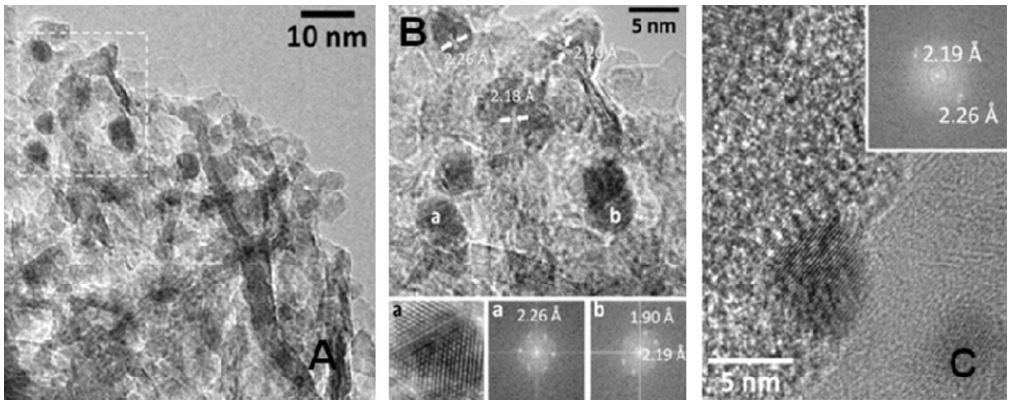

Fig. 9. TEM and lattice fringe images of sample R(0.5/0.5).

Catalyst R(0.5/0.5) (see Fig. 9) contains metal particles distributed in a narrow size interval of 5–7 nm in diameter. Fig. 9A shows a representative image; the area enclosed in the white square is shown in Fig. 9B under HRTEM conditions. Several particles exhibit lattice fringes and the FT images of two of them, labelled "a" and "b", are also included. On the basis of lattice spacing values, two type of particles are recognized: particles corresponding to Pt–Cu alloy with (1 1 1) crystallographic planes at 0.218–0.22 nm, and particles corresponding to pure Pt with (1 1 1) crystallographic planes at 0.226 nm. Apparently, Pt particles are slightly smaller than Pt–Cu alloy particles. The FT image of particle labelled "a" corresponds to a Pt crystallite oriented along the [1 1 0] crystallographic direction. The FT image of particle labelled "b" shows spots at 0.219 and 0.19 nm, which are ascribed to (1 1 1) and (2 0 0) planes of Cu and Pt, respectively. In Fig. 9C the HRTEM analysis reveals the occurrence of a two-domain particle. The corresponding FT image exhibits spots at 0.219 and 0.226 nm, which correspond to two well-defined domains in the same particle. The larger domain at 0.219 nm is ascribed to the (1 1 1) crystallographic planes of Pt–Cu alloy, whereas the small domain at 0.226 nm is ascribed to (1 1 1) planes of pure Pt. These observations suggest that after the first step of the preparation procedure, the catalyst is comprised by Pt–Cu alloy particles, and that after the second impregnation step, Pt particles are developed, some of them interacting with pre-existing Pt–Cu alloy.

A general view of the WR(0.5/0.5) is shown in Fig. 10A. Particles ranging in size from 1.5 and 8.0 nm are encountered with different composition. As a general rule, larger particles are pure Cu crystallites whereas smaller ones are mainly pure Pt. Pt–Cu alloy particles are also identified on the basis of lattice fringe analysis. Fig. 10B shows an individual particle with lattice spacing at 0.218 nm, which is ascribed to the (1 1 1) crystallographic plane of Pt–Cu. Fig. 10C shows a large particle with lattice fringes at 0.209 nm, which correspond to (1 1 1) crystallographic planes of pure Cu.

Table 5
Metal particle size and type of Pt–Cu interaction of the catalysts determined by HRTEM.

Sample	Particle size range (nm)	Phases detected
R(0.5)	1.8–2.4	Pt–Cu alloy and Cu particles
R(1)	2.1–4	Pt–Cu alloy and Cu particles
R(0.5/0.5)	5–7	Pt–Cu alloy and Pt and Cu particles
WR(0.5)	1.4–4	Cu and Pt particles in close contact
WR(1)	5–10	Cu and Pt particles in close contact and a limited extent of Pt–Cu alloy
WR(0.5/0.5)	1.5–8	Pt–Cu alloy and Pt and Cu particles

Using protocol DI we obtained different surfaces depending on the parent catalysts used and different interaction were achieved.

A higher Pt metal loading leads to a higher metallic particle size for catalyst prepared by protocols R and WR. WR-type catalysts present bigger and broader particle size compared to their analogous R-type catalyst.

Table 5 presents a summary of the HRTEM for each catalyst.

Some of the samples were also analyzed after reaction by HRTEM. The main phase detected for all the catalysts was CuO (as confirmed by XRD). Fig. 11A shows a low-magnification image of WR(0.5) used catalyst. Apparently, there is some extent of rehydration (as confirmed by XRD and FTIR) as well as some compaction with respect to the fresh sample. Fig. 11B shows another area of the sample. Again, rehydration is apparent and, in this case, metal particles with a higher electron contrast are evident, ranging from

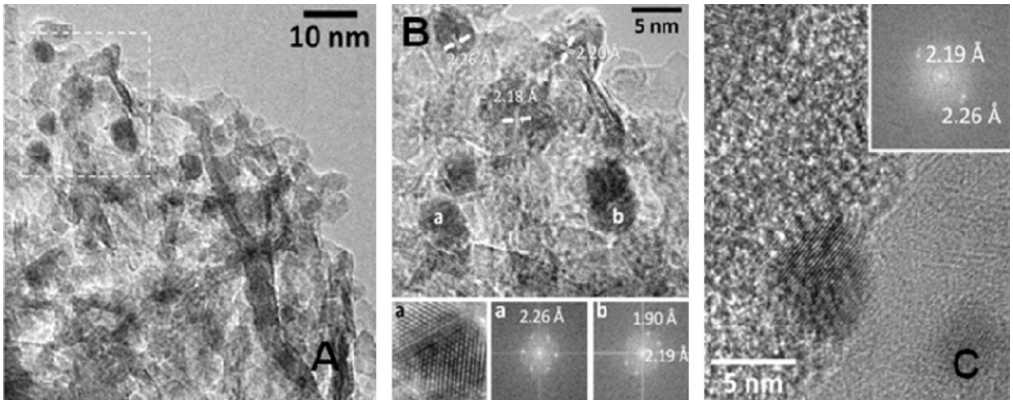

Fig. 10. TEM and HRTEM images of sample WR(0.5/0.5).

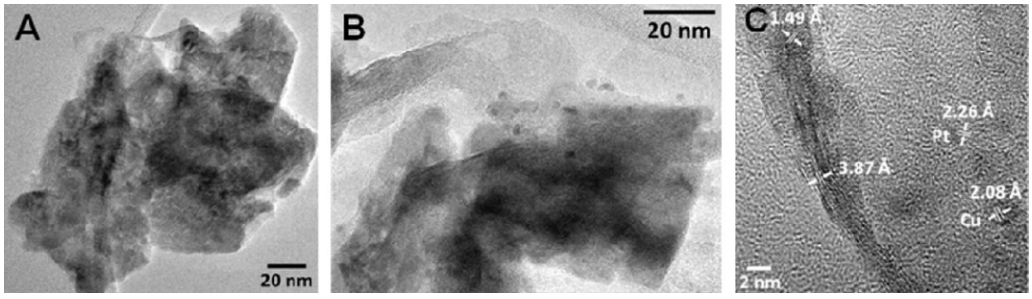

Fig. 11. TEM and HRTEM image of WR(0.5) used catalyst.

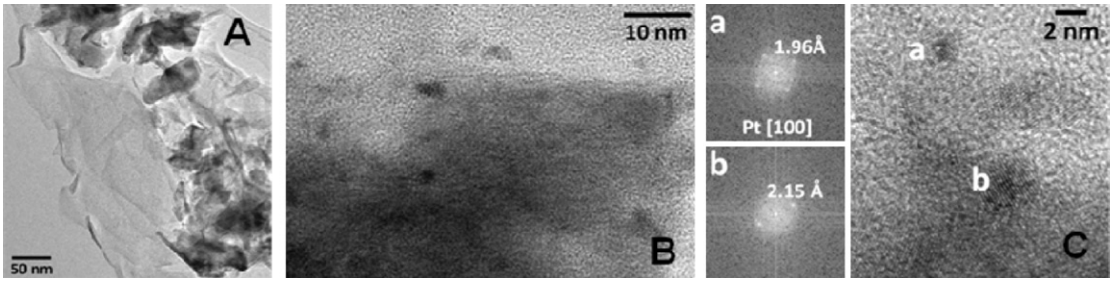

Fig. 12. TEM and HRTEM image of WR(0.5/0.5) used catalyst.

about 2 to 8 nm in size. A detailed lattice fringe image is depicted in Fig. 11C. In the image three different types of particles are recognized. Intense lattice fringes at 0.387 nm are indicative of (0 0 6) crystallographic planes of the rehydrated phase, which may also account for the lattice fringes at 0.149 nm (1 1 3). Metal particles fall in two categories; those ranging from 4 to 8 nm exhibit lattice fringes of metallic copper, like those at 0.208 nm in Fig. 11C, which are ascribed to (1 1 1) planes of Fm3m Cu. Smaller metal particles of about 2 nm in size show lattice fringes corresponding to metallic Pt. This is indicated in Fig. 11C for the particle with lattice fringes at 0.226 nm, which correspond to (1 1 1) planes of cubic Pt.

A general view of WR(0.5/0.5) used catalysts is shown in Fig. 12A. Rehydration is evident in the form of layered structures all over the sample. More compact aggregates and well dispersed nanoparticles are also evident in the image. These nanoparticles range from ca. 2 to 6 nm in size (see Fig. 12B as an example). A detailed analysis of the nature of these nanoparticles has been carried out in high resolution mode. Fig. 11C shows a lattice fringe image and two Fourier Transform (FT) images of individual crystallites labelled "a" and "b". Crystallite "a" measures ca. 1.9 nm and exhibits crystallographic planes at 0.196 nm. These are characteristic of (2 0 0) planes of metallic platinum; the relative distances of spots in the FT image reveals that the Pt particle is oriented along the [1 0 0] crystallographic direction. Particle "b", which measures 5.5 nm, exhibits lattice fringes at 0.215 nm. This spacing is intermediate between (1 1 1) planes of Fm3m Pt (0.226 nm) and Cu (0.209 nm), thus pointing to the occurrence of a Pt–Cu alloy, as it was observed in the fresh sample. Therefore, besides rehydration, the sample after reaction contains three types of metal particles, small ones (about 2 nm) of pure Pt, Pt–Cu alloy particles of about 5–6 nm, and like all the used samples Cu particles, which is fairly similar to the sample before reaction.

Fig. 13A shows a general view of the R(1) used catalyst, which contains metallic particles with a narrow size distribution centered at about 2–4 nm. In R(1) used catalyst, rehydration is less evident with respect to the preceding samples. Lattice fringe analysis reveals that in all cases, metallic particles are Pt–Cu alloy. As an example, Fig. 13B depicts one of these nanoparticles, which exhibits lattice fringes at 0.218 nm, characteristic of a Pt–Cu alloy. Another representative image is shown in Fig. 13C, where two of these nanoparticles exhibit lattice fringes at 0.216–0.218 nm, indicating that Pt–Cu alloys of different composition occur in the sample. No isolated Pt particles have been identified by HRTEM.

In conclusion, after the catalytic tests the particle size distribution and the type of active sites in the catalysts remain similar to the initial catalysts and some oxidation of the copper and rehydration of the mixed oxide is observed, but according to H_2-TPR results the quantity of the active sites (mainly related to copper) changed.

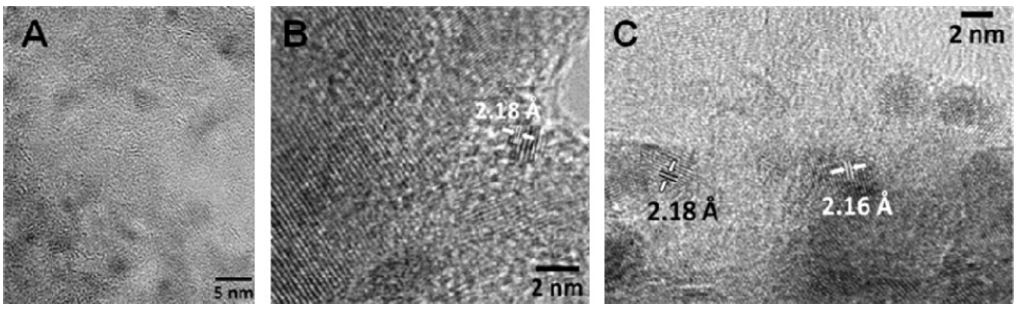

Fig. 13. TEM and HRTEM image of R(1) used catalyst.

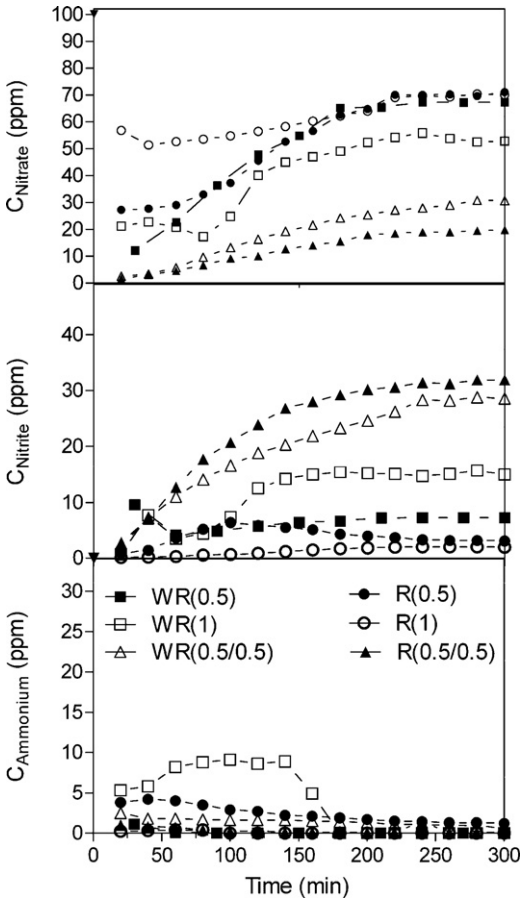

Fig. 14. Concentration vs. time in continuous catalytic tests done with 1 g of catalysts.

3.2. Catalytic activity

Fig. 14 shows the nitrate, nitrite and ammonium concentrations during the reaction in the test performed with 1 g of catalysts. Similar profiles are observed for test performed with 0.5 g of catalysts.

It is observed in Fig. 14 that catalysts present initial deactivation, and the steady state is achieved at around 300 min of reaction time, when the nitrate, nitrite and ammonium concentrations in time are practically constant. The initial deactivation observed could be mainly due to: (i) metal leaching, and/or (ii) adsorption effects at initial time, and/or (iii) the oxidation of copper that is not in contact with Pt and then not regenerated by the noble metal as evidenced by H_2-TPR. The copper concentration in water after treatment in the catalytic test was analyzed by atomic absorption to evaluate the stability of the catalysts. The copper concentration was less than 13 ppb in all cases, therefore under the potable water limitations (2 ppm) of the European Union [47]. No leaching of Pt was detected during the experiments. The catalysts leaching is negligible and do not have important contribution to the initial deactivation.

In order to study the adsorption effect on the catalytic activity, three blank tests were performed (Section 2.3); the results are presented in Fig. 15. The catalytic activity of the CuMgAl support was tested as reference material (as monometallic catalyst). The sample was reduced at 300 °C under hydrogen flow, and then tested at the same conditions described for the catalytic tests (Test 1). As observed in Fig. 15, the support presents a decreasing nitrate reduction activity, and at 300 min a remaining nitrate removal of 11% is detected. A total deactivation of the catalysts is not observed due to the high Cu content. This corroborates that nitrate can be reduced on copper monometallic sites, but the catalytic activity is

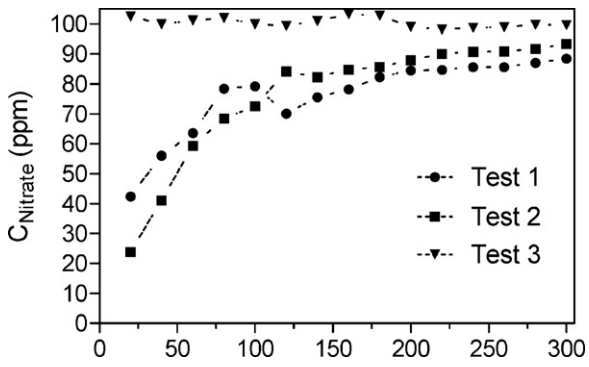

Fig. 15. Tests for the determination of catalytic and adsorption capacity of CuMgAl support.

very low, in agreement with previous investigations [29,44]. It is generally accepted that Cu monometallic sites are not stable for nitrate reduction, and the results confirm that the presence of a noble metal (like Pt) is necessary to maintain the catalytic activity. No ammonium formation is detected obtaining nitrites as the main species.

Considering that calcined hydrotalcite-type materials have memory effect, their adsorption capacity for nitrates was also studied (Tests 2 and 3). In Test 2 the same conditions as Test 1 were applied, but no hydrogen was fed to the reactor. A high initial activity and a similar concentration profile to Test 1 were observed. The nitrate removal rate decreases rapidly in time due to surface oxidation of copper, until 6% at 300 min of reaction time transforming nitrate to nitrite. In hydrotalcite-based catalysts for the nitrate reduction, there is an intrinsic relation between adsorption and catalytic activity as previously proposed by Palomares et al. [33] in a reaction mechanism that involve nitrate and nitrite in the interlayer space, due to the reconstruction ability of these materials. This effect is weaker in the catalysts used in the present study due to the high copper content that diminish the reconstruction ability (evidenced by the weak and amorphous peaks characteristic of HT material in the XRD patterns of used catalysts). With these previous results, we could consider that when the catalytic system achieves the steady state (around 300 min) there is not real adsorption of nitrate or nitrite, probably due to the high copper content that avoid the recovering of the initial hydrotalcite phase. A third test was performed (Test 3). In this test the adsorption capacity of the support (without reduction) was studied. No nitrate removal or nitrite production is observed. This confirms that the contribution of nitrate removal due to adsorption in the support can be neglected. Therefore, the stability of the catalysts could be related to the changes of the active phases evidenced by H_2-TPR profiles, HRTEM and XRD results of the used samples. The presence of copper oxide phase after reaction could explain the catalyst deactivation.

3.2.1. Nitrate conversion

It is well established that the nitrate conversion depends on different variables such as: nature of the metal in the surface, metal dispersion, bimetallic pair [46], reduction conditions [37], catalysts preparation method, among others. In this study we particularly analyzed the influence of: (i) the Pt–Cu alloy formation and (ii) the Pt metal loading, in the nitrate conversion. Fig. 16 presents the conversions for two different catalyst weights (0.5 and 1.0 g).

The conversion varies strongly with the synthesis protocol. Firstly, as for the one-step impregnation protocols, it is observed that WR(0.5) and WR(1) catalysts achieved higher nitrate conversions than their analogous R-type catalysts (R(0.5) and R(1)) at the same catalysts weight. This could be related to: (i) the decrease of metal surface area due to sintering of Cu particles involved in

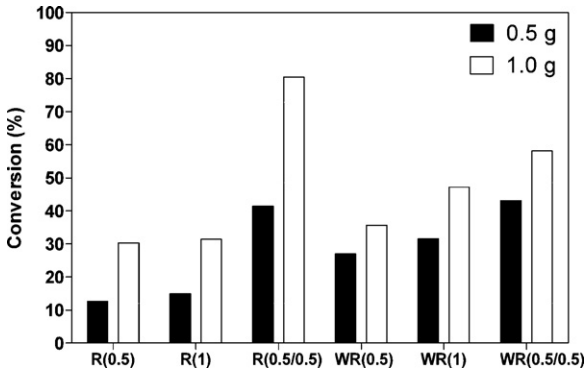

Fig. 16. Nitrate conversion at 300 min for the different catalyst amounts in the reactor bed.

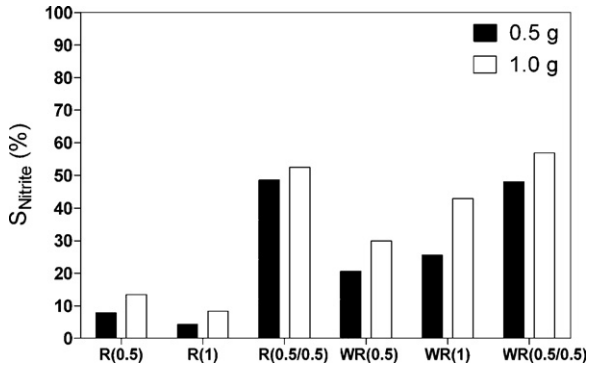

Fig. 17. Nitrite selectivity at 300 min for the different catalysts weights.

protocol R and/or (ii) the type of metallic sites detected on the surface by HRTEM. The metallic particle sizes in R-type catalysts are smaller than WR-type catalysts (see HRTEM results) so the first possibility can be discarded. Based on the previous HRTEM results on these samples, we can suggest that a combination of mainly isolated Cu and Pt particles on the surface with some extent of Cu–Pt alloy particles (WR(0.5) and WR(1)) enhance the nitrate conversion compared to the combination of Cu and Pt–Cu alloy particles (R(0.5) and R(1)). These results are in agreement with those of Soares et al. [37] showing that high activities were obtained when the metals were in close contact but not alloyed.

Secondly, it is observed that catalysts prepared by Protocol DI (WR(0.5/0.5) and R(0.5/0.5)) present higher conversion compared to WR(1) and R(1) catalysts. Double impregnation protocol enhances the nitrate conversion compared to one step impregnation protocols with the same Pt content (1%wt). It is noteworthy that in contrast to one step impregnated catalysts (R(1) vs. WR(1)), R(0.5/0.5) exhibit higher conversion than WR(0.5/0.5) when the reaction is performed with 1 g of catalyst. This could be related to the surface metal chemistry but the magnitude differs with the parent catalyst. It seems that Pt particles formed during the second impregnation step interacting with pre-existing Pt–Cu alloy particles (observed by HRTEM in R(0.5) and in some extent in WR(0.5)) and with isolated Cu particles enhance strongly the conversion. Consistently, the effect is enhanced in R(0.5/0.5) because the parent catalyst presented higher amount of Pt–Cu alloy particles. This can also explain that WR-type catalysts impregnated once present higher nitrate conversion. They possess this kind of active sites but in fewer amounts compared to the catalysts impregnated twice.

Different Pt metal loadings (0.5% and 1%Pt) were tested, but this variable does not affect the nitrate conversion considerably. This fact was previously observed in analogous Pt/CuZnAl catalysts [44]. It seems that the Cu–Pt interaction does not change with the Pt metal loading in the range studied (as it was observed by HRTEM). A higher Pt content and other synthesis methods should be tried in order to cause a different interaction between the metals as it was previously reported [49]. Also it would be interesting to co-precipitate Pt precursor during the HT synthesis to favor Pt–Cu interaction.

In conclusion, in view of the obtained results to maximize the nitrate conversion it is necessary to obtain mainly Pt–Cu alloy particles interacting with Pt particles in the surface of the catalysts.

3.2.2. Selectivity

The synthesis protocol has also a strong effect on the reaction selectivity toward the intermediate nitrite as well as on the final products (NH_4^+ and N_2). The catalytic results are explained considering the differences in the type of predominant metal particles at the surface of the catalysts determined by HRTEM.

3.2.2.1. Nitrite selectivity. Nitrite is an intermediate product of the nitrate reduction [42,44]. Fig. 17 shows the nitrite selectivity for the different synthesis protocols and catalysts weights. It is observed that the conversion level and the synthesis protocol affect the nitrite selectivity.

Considering the same synthesis protocol, it is observed that the conversion and nitrite selectivity increase with the catalysts weight, confirming that the nitrate reduction rate is faster than the nitrite hydrogenation rate, as previously reported by Wang et al. [28]. While considering the different types of protocols, (Fig. 18) the increase of the nitrite selectivity with WR-type catalysts follows the increase in conversion, but differs with the catalyst weight. The same tendency is not observed for R-type catalysts probably due to the intermediate reduction step in the synthesis protocol.

The nitrite selectivity, related to the conversion, also depends on the synthesis protocol of the catalysts. Comparing the one step impregnated catalysts, it could be said that WR(0.5) and WR(1) samples present higher nitrite selectivity than R(0.5) and R(1). Considering the same conversion level of 30%, the nitrite selectivity is around 13% and 30% for R(0.5) and WR(0.5), respectively (for 1 g of catalyst). It seems that a major presence of Pt–Cu alloy particles present in R(0.5) and R(1) improves nitrite reduction compared to the Cu and Pt isolated particles mainly observed in samples WR(0.5) and WR(1).

Regarding the samples impregnated twice, the nitrite selectivity is also affected by the synthesis protocol and the nitrate conversion. Samples R(0.5/0.5) and WR(0.5/0.5) present a significantly higher nitrite selectivity than sample R(1). The nitrite selectivity reaches 48% for R(0.5/0.5) and WR(0.5/0.5), whereas it is 42% and 9% for WR(1) and R(1), respectively, at similar conversion levels around 43%. This confirm that Pt–Cu alloy particles decrease the nitrite selectivity compared to the combination of Pt and

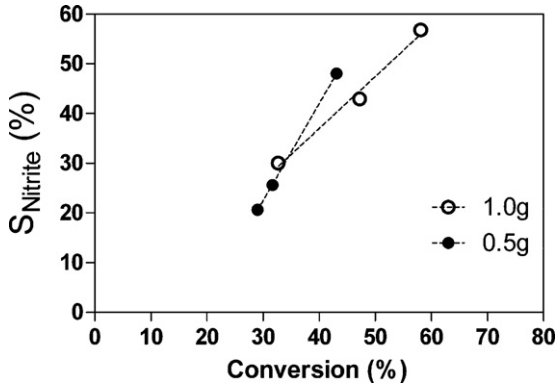

Fig. 18. Nitrite selectivity vs. conversion for WR-type catalysts at different catalyst weights.

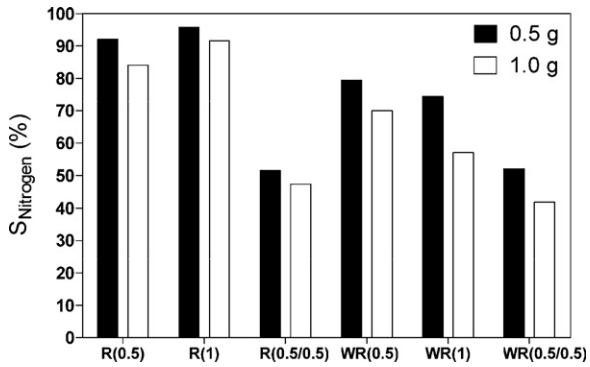

Fig. 19. Nitrogen selectivity at 300 min for the different catalysts weights.

pre-existent Pt–Cu alloy particles present in the samples impregnated two times.

With respect to the Pt content, it does not affect significantly the nitrite selectivity, likely related to the conversion. A slightly lower nitrite selectivity in R(1) compared to R(0.5) sample could account for a more homogeneous formation of Pt–Cu alloy particles described in the HRTEM section.

As a conclusion, Pt–Cu alloy particles allow to decrease nitrite formation as intermediate product. Nitrite concentration needs to be improved to fulfill the maximum admissible concentration of the EU legislation (0.3 ppm) [2].

3.2.2.2. Ammonium selectivity. Ammonium was detected in low concentrations under the maximum admissible in potable water (0.3 ppm) according to the E.U legislation [2]. These values are considerably lower than those obtained by similar Pd–Cu/Mg/Al catalysts [33] at the same conversion and similar to Pt/CuZnAl catalysts [44]. In all cases ammonium selectivity lower than 5% was achieved and due to these low values it is not possible to establish a direct relation with the surface metal state. The low selectivity could be related to: (i) the low platinum content compared to copper content in all samples, this possibly affected the hydrogenation ability of Pt [35,48] avoiding deeply hydrogenated of nitrate into ammonium [49], (ii) to the low conversion levels and/or (iii) due to the OH^- control by the HT support [33] (during the tests in the continuous reactor the pH was lower than 8).

3.2.2.3. Nitrogen selectivity. Fig. 19 shows the nitrogen selectivity achieved by the catalysts. In this case, due to the low ammonium selectivity and considering Eq. (3), it could be said that the catalysts with the lowest nitrite selectivity have the highest nitrogen selectivity ($S_{Nitrogen} \approx 100 - S_{Nitrite}$); subsequently the active sites that enhance the nitrite reduction also enhance the nitrogen selectivity.

It is concluded that the nitrogen selectivity is enhanced by the Pt–Cu alloy formation.

4. Conclusions

Pt/CuMgAl calcined HT catalysts are active catalysts for nitrate reduction in water. Different Pt impregnation protocols were used, leading to different surface phases that were related to the catalytic activity and selectivity to nitrogen. The main conclusions are:

- To maximize the nitrate conversion it is necessary to obtain mainly Pt particles interacting with Cu and Pt–Cu alloy particles; this is achieved by double Pt impregnation protocols.
- Pt–Cu alloy active sites seem to favor the nitrogen selectivity and the nitrite reduction as an intermediate product, but the nitrate conversion is negatively affected.
- If Cu and Pt particles are mainly isolated, the nitrate conversion is maintained probably by hydrogen spillover, but it is not the best configuration to maximize conversion and nitrogen selectivity.
- It is necessary to diminish nitrite concentration and to further enhance the nitrogen production for this kind of catalysts.

Acknowledgments

Authors are grateful to Universitat Rovira i Virgili, the Spanish Ministry of Science and Innovation (Ramon y Cajal Program funding S.C. and project CTQ2009-12520) and Project 2008ITT-CTP-00111 for funds received to carry out this work. With the support of the "Comisionado para Universidades e Investigación del Departamento de Innovación, Universidades y Empresa de la Generalitat de Cataluña" and European Social Fund. F. Medina and J. Llorca acknowledge Generalitat de Catalunya for ICREA ACADEMIA award and N. Barrabés for financial support by Marie Curie project (PIEF-GA-2009-236741 – ENVIROCATHYDRO).

References

[1] L.W. Canter, Nitrates in Groundwater, CRC Press, Boca Raton, 1996.
[2] European Communities (Drinking Water) (No. 2), Regulations 2007. Statutory instruments.
[3] Health Canada, Guidelines for Canadian Drinking Water Quality, sixth ed. Ministry of Health, Ottawa, 1996.
[4] K.M. Hiscock, J.W. Lloyd, D.N. Lerner, Water Res. 25 (1991) 1099–1111.
[5] A. Kapoor, T. Viraraghavan, A. Fellow, J. Environ. Eng. (Reston, VA, U.S.) 123 (1997) 371–380.
[6] M. Shrimali, K.P. Singh, Environ. Pollut. 112 (2001) 351–359.
[7] N. Barrabés, A. Dafinov, F. Medina, J.E. Sueiras, Catal. Today 149 (2010) 341–347.
[8] G. Centi, S. Perathoner, Appl. Catal. B 41 (2003) 15–29.
[9] J.N. Cevaal, W.B. Suratt, J.E. Burke, Desalination 103 (1995) 101–111.
[10] J.B. de Heredia, J.R. Dominguez, Y. Cano, I. Jimenez, Appl. Surf. Sci. 252 (2006) 6031–6035.
[11] M.I.M. Soares, Water, Air, Soil Pollut. 123 (2000) 183–193.
[12] J.P. van der Hoek, A. Klapwijk, Water Res. 21 (1987) 989–997.
[13] U. Prusse, M. Hahnlein, J. Daum, K.-D. Vorlop, Catal. Today 55 (2000) 79–90.
[14] K.-D. Vorlop, T. Tacke, Chem. Ing. Tech. 61 (1989) 836–837.
[15] F.A. Marchesini, S. Irusta, C. Querini, E. Miro, Catal. Commun. 9 (2008) 1021–1026.
[16] N. Barrabés, J. Just, A. Dafinov, F. Medina, J.L.G. Fierro, J.E. Sueiras, P. Salagre, Y. Cesteros, Appl. Catal. B 62 (2006) 77–85.
[17] A. Garron, K. Lazar, F. Epron, Appl. Catal. B 59 (2005) 57–69.
[18] D. Gasparovicová, M. Králik, M. Hronec, Z. Vallusová, H. Vinek, B. Corain, J. Mol. Catal. A: Chem. 264 (2007) 93–102.
[19] J. Sá, H. Vinek, Appl. Catal. B 57 (2005) 247–256.
[20] J. Sá, D. Gasparovicova, K. Hayek, E. Halwax, J.A. Anderson, H. Vinek, Catal. Lett. 105 (2005) 209–217.
[21] Y. Sakamoto, K. Nakamura, R. Kushibiki, Y. Kamiya, T. Okuhara, Chem. Lett. 34 (2005) 1510–1511.
[22] D. Wan, H. Liu, X. Zhao, J. Qu, S. Xiao, Y. Hou, J. Colloid Interface Sci. 332 (2009) 151–157.
[23] N. Barrabés, J. Sá, Appl. Catal. B: Environ. 104 (2011) 1–5.
[24] A.J. Lecloux, Catal. Today 53 (1999) 23–34.
[25] A. Pintar, J. Batista, Catal. Today 53 (1999) 35–50.
[26] U. Prüsse, K.-D. Vorlop, J. Mol. Catal. A: Chem. 173 (2001) 313–328.
[27] Y.-X. Chen, Y. Zhang, G.-H. Chen, Water Res. 37 (2003) 2489–2495.
[28] Y. Wang, J. Qu, H. Liu, J. Mol. Catal. A: Chem. 272 (2007) 31–37.
[29] F. Epron, F. Gauthard, C. Pinéda, J. Barbier, J. Catal. 198 (2001) 309–318.
[30] U. Prusse, S. Horold, K.D. Vorlop, Chem. Ing. Tech. 69 (1997) 93–97.
[31] F. Gauthard, F. Epron, J. Barbier, J. Catal. 220 (2003) 182–191.
[32] A.E. Palomares, J.G. Prato, F. Márquez, A. Corma, Appl. Catal. B 41 (2003) 3–13.
[33] A.E. Palomares, J.G. Prato, F. Rey, A. Corma, J. Catal. 221 (2004) 62–66.
[34] J. Sá, T. Berger, K. Föttinger, A. Riss, J.A. Anderson, H. Vinek, J. Catal. 234 (2005) 282–291.
[35] Y. Yoshinaga, T. Akita, I. Mikami, T. Okuhara, J. Catal. 207 (2002) 37–45.
[36] F. Deganello, L.F. Liotta, A. Macaluso, A.M. Venezia, G. Deganello, Appl. Catal. B 24 (2000) 265–273.
[37] O.S.G.P. Soares, J.J.M. Órfão, J. Ruiz-Martínez, J. Silvestre-Albero, A. Sepúlveda-Escribano, M.F.R. Pereira, Chem. Eng. J. (Lausanne) 165 (2010) 78–88.
[38] Y. Matatov-Meytal, V. Barelko, I. Yuranov, M. Sheintuch, Appl. Catal. B 27 (2000) 127–135.
[39] N. Barrabés, D. Cornado, K. Foettinger, A. Dafinov, J. Llorca, F. Medina, G. Rupprechter, J. Catal. 263 (2009) 239–246.
[40] F. Cavani, F. Trifirò, A. Vaccari, Catal. Today 11 (1991) 173–301.

[41] M. Turco, G. Bagnasco, C. Cammarano, P. Senese, U. Costantino, M. Sisani, Appl. Catal. B 77 (2007) 46–57.
[42] Y. Wang, J. Qu, H. Liu, C. Hu, Catal. Today 126 (2007) 476–482.
[43] Y. Wang, J. Qu, H. Liu, R. Wu, Chin. Sci. Bull. 51 (2006) 1431–1438.
[44] A. Aristizábal, M. Kolafa, S. Contreras, M. Domínguez, J. Llorca, N. Barrabés, D. Tichit, F. Medina, Catal. Today. 2011, doi:10.1016/j.cattod.2011.02.044, in press.
[45] O.S.G.P. Soares, J.J.M. Órfão, M.F.R. Pereira, Catal. Lett. 139 (2010) 97–104.
[46] S. Kannan, V. Rives, H. Knözinger, J. Solid State Chem. 177 (2004) 319–331.
[47] EEC-European Economic Community, The Drinking Water Directive (DWD) Council Directive 98/83/EC, concerns the quality of water intended for human consumption, 1998, p. Annexe I. Part B.
[48] R. Mélendrez, G. Del Angel, V. Bertin, M.A. Valenzuela, J. Barbier, J. Mol. Catal. A: Chem. 157 (2000) 143–149.
[49] O.S.G.P. Soares, J.J.M. Órfão, M.F.R. Pereira, Appl. Catal. B: Environ. 91 (2009) 441–448.